Vol 446|26 April 2007|doi:10.1038/nature05733

LETTERS

# How swifts control their glide performance with morphing wings

D. Lentink[1], U. K. Müller[1], E. J. Stamhuis[2], R. de Kat[3], W. van Gestel[1], L. L. M. Veldhuis[3], P. Henningsson[4], A. Hedenström[4], J. J. Videler[2,5] & J. L. van Leeuwen[1]

**Gliding birds continually change the shape and size of their wings[1–6], presumably to exploit the profound effect of wing morphology on aerodynamic performance[7–9]. That birds should adjust wing sweep to suit glide speed has been predicted qualitatively by analytical glide models[2,10], which extrapolated the wing's performance envelope from aerodynamic theory. Here we describe the aerodynamic and structural performance of actual swift wings, as measured in a wind tunnel, and on this basis build a semi-empirical glide model. By measuring inside and outside swifts' behavioural envelope, we show that choosing the most suitable sweep can halve sink speed or triple turning rate. Extended wings are superior for slow glides and turns; swept wings are superior for fast glides and turns. This superiority is due to better aerodynamic performance—with the exception of fast turns. Swept wings are less effective at generating lift while turning at high speeds, but can bear the extreme loads. Finally, our glide model predicts that cost-effective gliding occurs at speeds of 8–10 m s$^{-1}$, whereas agility-related figures of merit peak at 15–25 m s$^{-1}$. In fact, swifts spend the night ('roost') in flight at 8–10 m s$^{-1}$ (ref. 11), thus our model can explain this choice for a resting behaviour[11,12]. Morphing not only adjusts birds' wing performance to the task at hand, but could also control the flight of future aircraft[7].**

Bird wings lend themselves to morphing because they have an articulated skeleton under muscular control, and because the changing overlap between feathers allows continuous changes in wing shape and wing size. Gliding birds sweep their hand-wings back at high flight speeds[1–5,13], and spread their wings in turns[4]. To test whether a bird's chosen wing geometry maximizes its flight performance, biologists have focused on gliding flight[1–5,13], during which changes in wing geometry are not related to wing beat. Aerodynamic forces have been inferred from the behaviour of freely gliding birds[1,2,5,13]; lift and drag have also been measured directly on single bird wings fixed in one shape[14,15]. These approaches provide no information on morphing outside the bird's behavioural envelope, and must be supplemented with aerodynamic theory in order to predict wing aerodynamic performance and bird glide performance[2,16,17].

Rather than estimating how wing geometry affects wing performance, we measured it in a wind tunnel. We chose the common swift (*Apus apus*), which spends most of its life on the wing, foraging, courting, migrating and even roosting[11,12,18,19], and has a gliding repertoire to suit: soaring, gliding and 'flap-gliding'. Flap-gliding birds alternate flapping and gliding at 1–2 s intervals[11,19], matching the speeds of flapping and gliding episodes[20]. With speed approximately constant, glides can be approximated as 'equilibrium gliding', which encompasses turns and straight glides (turns with infinite radius) (Fig. 1; Methods). During this steady state, flight performance can be deduced from four readily measured parameters: aerodynamic lift, drag, body mass, and flight velocity (Fig. 1b). These determine the swift's glide path, conventionally described by glide angle, turning radius, and bank angle[21]. Glide path and velocity determine bird glide performance.

Aerodynamic force is proportional to force coefficient × wing area × square of glide speed[21]. Swifts control force coefficient by altering wing shape, angle of attack, and speed. Increasing sweep angle from 5° (fully extended) to 50° (Fig. 2a) decreases wing area and shape (that is, aspect ratio) by roughly one-third (Fig. 2b, c). We quantified how variable sweep affects wing aerodynamics by measuring

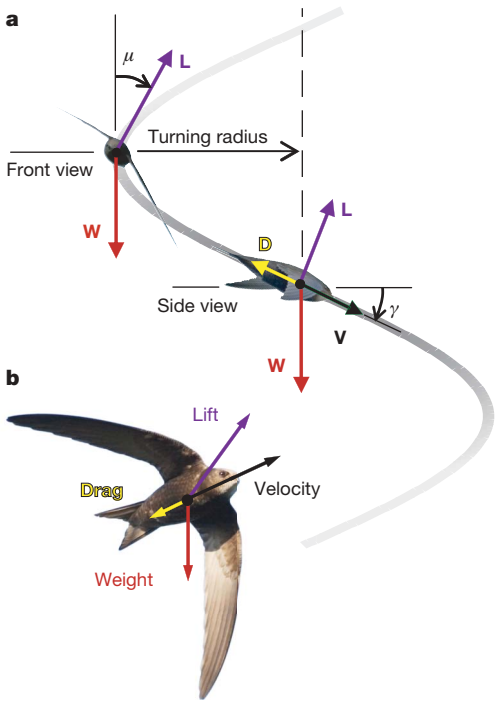


**Figure 1 | Equilibrium gliding along a helical path. a**, Turning swifts glide at a constant glide speed, whereas glide velocity ($V$) changes direction along a helical path (grey ribbon) inclined downward at glide angle $\gamma$. To turn without sideslip, swifts incline sideways at bank angle $\mu$. Glide angle is determined by the cos$\mu$ component of lift divided by drag, while the sin$\mu$ component of lift provides the centripetal force required for turning. **L**, lift; **D**, drag; **W**, weight. **b**, Main forces acting on a swift gliding at a given velocity.

[1]Experimental Zoology Group, Wageningen University, 6709 PG Wageningen, The Netherlands. [2]Department of Marine Biology, Groningen University, 9750 AA Haren, The Netherlands. [3]Department of Aerospace Engineering, Delft University of Technology, 2629 HS Delft, The Netherlands. [4]Department of Theoretical Ecology, Lund University, Ecology Building, SE-223 62 Lund, Sweden. [5]Institute of Biology, Leiden University, 2300 RA Leiden, The Netherlands.

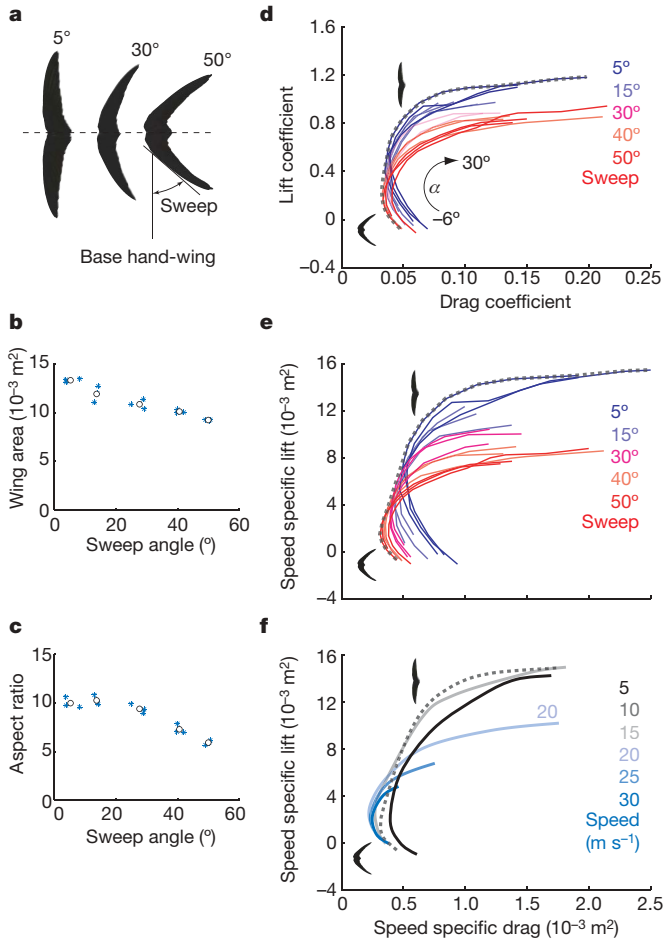


**Figure 2 | Morphing swift wings can generate higher lift and lower drag than wings with a fixed geometry.** **a–c**, Adjusting sweep angle (**a**) alters wing area (**b**) and aspect ratio (**c**). Blue stars, individual wings; open circles, average per sweep. **d**, The enveloping polar (grey dashed line) spans a wider range of lift and drag coefficients than the polar for any one sweep (fine coloured lines) (angles of attack $\alpha$, $-6^\circ$ to $+30^\circ$; glide speed, 10 m s$^{-1}$). **e**, The combined effect of wing shape and size (speed-specific lift and drag[22]) further enlarges the enveloping polar. **f**, Increasing glide speed shifts enveloping polars to the left, and decreases maximum speed-specific lift.

lift and drag on 15 wing pairs in the Delft low-turbulence wind tunnel (see Methods).

Our experiments show that variable sweep enlarges the aerodynamic performance envelope of swift wings. At a given glide speed, the 'polars' of lift versus drag coefficient (Fig. 2d) for individual sweep angles build up to a much wider enveloping polar: swept wings contribute low drag coefficients at low angles of attack; extended wings contribute high lift coefficients at high angles of attack. The effects of wing shape are 'amplified' by wing area (Fig. 2e plots the same data as polars of speed-specific lift and drag[22]; that is, lift coefficient × wing area versus drag coefficient × wing area). The decrease in wing area with increasing sweep further enlarges the enveloping polar for a given glide speed, further widening the performance gap between fixed-shape and morphing wings.

The enveloping polar changes with glide speed (Fig. 2f). With increasing speed, the polar at first maintains its shape and shifts to lower drag values[10,23] because drag coefficient scales with speed to a power less than two at low angles of attack, when flow separation is minimal[24]. Beyond 15 m s$^{-1}$, the enveloping polar breaks off at lower and lower speed-specific lift values because less swept wings break under the extreme loads; only the more swept wings are left to build up the enveloping polar.

To demonstrate how morphing wings can affect gliding, we translated the above measures of wings' aerodynamics into swift's flight-dynamics—our six figures of merit (see Supplementary equations). Three flight-cost related indices are: (1) glide distance (expressed as the maximum glide ratio[21]), (2) glide duration[21], and (3) turn angle for a given height loss. By maximizing distance or time spent gliding, birds reduce energy expenditure while foraging and roosting. Three indices are agility-related: pursuits and escapes require (4) fast turns (high angular velocity[21]) with (5) a high path curvature[21]; while (6) high horizontal speed (the horizontal component of glide velocity) helps to avoid drift in strong winds. Our discussion of performance maxima ignores combinations of sweep and glide speed that cause diving (glide angles >45°, Fig. 1).

Extended wings provide the best glide performance. Five of the six indices (Fig. 3a, b, d–f) reach an absolute maximum with extended wings—characteristic of gliders in general. The cost-related maxima occur between 8 and 15 m s$^{-1}$. At 10 m s$^{-1}$, within this optimal speed range, choosing extended over swept wings triples all three turning indices (Supplementary Fig. 2). Nevertheless, swifts sometimes choose higher glide speeds[11,18].

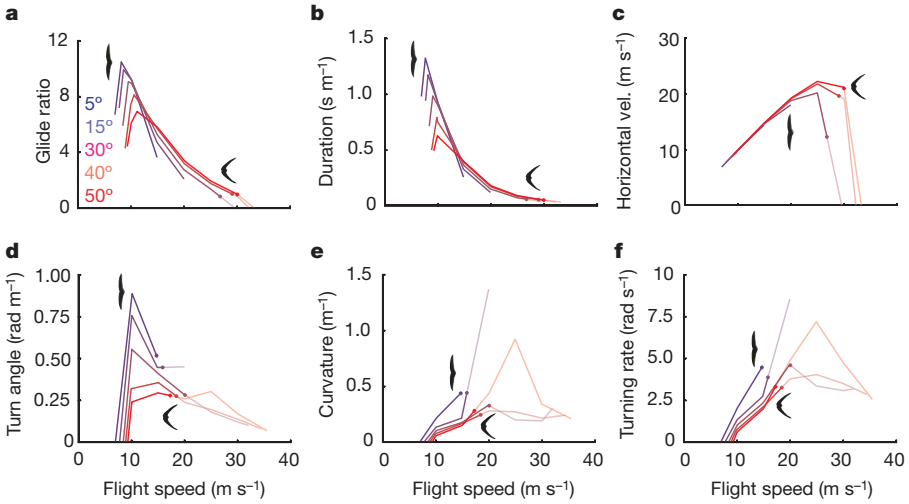


**Figure 3 | Morphing improves glide performance of swifts.** **a–f**, Performance indices for a range of sweep angles (coloured lines) and flight speeds ($x$ axis). Absolute performance maxima occur at low speeds and sweeps in all indices except horizontal velocity, **c**. In two of three straight-flight indices (top row), low sweep delivers superior performance at low speeds while high sweep is superior at high speeds. During turning (bottom row), no crossover from low to high sweep occurs during gliding. Solid lines, glide angle < 45°; dot, glide angle = 45°; no dot, wing fails before 45° is reached; faint lines, glide angle > 45°.

During straight glides at higher-than-optimal speeds, high sweep improves aerodynamic wing performance. Consider Fig. 3a: at lower-than-optimal speeds (left of highest peak), extended wings deliver superior glide ratios. As speed increases beyond the optimum, the lines of constant sweep cross, and glide ratio is higher for swept wings. At 20 m s$^{-1}$, for example, a sweep angle of 50° yields a 70% improvement over extended wings, whereas at speeds below 10 m s$^{-1}$, extended wings improve glide ratio by as much as 50%. The second cost-related index, glide duration, behaves similarly (Fig. 3b). Unsurprisingly, 'horizontal speed' is the only index that peaks at high glide speeds (Fig. 3c). Although not sensitive to sweep angle at low glide speeds, horizontal speed increases with increasing sweep above 20 m s$^{-1}$. These results confirm predictions that swept wings improve glide performance at high speed[2,6].

Swept wings can bear higher loads during fast turns. Whereas, during straight gliding at constant speed, the wings bear a load necessarily equal to the bird's mass × 1*g*, centripetal acceleration increases the load during equilibrium turns. If the bird were to maximize aerodynamic wing performance, it should choose low sweep and low speed: the superior lift force of extended wings is desirable at any speed, in theory[16]. Consistent with this prediction, our measurement-based turning indices show no clear crossovers from low to high sweeps at glide angles below 45° (Fig. 3d–f). Dive performance (glide angle >45°) is severely limited during high-speed turns due to high loads. We measured loads of up to six times the bird's weight (Fig. 4 bottom), and observed two types of structural failure: one extended-wing specimen bent to the point of breaking at 15 m s$^{-1}$; another started vibrating violently at 15 and 20 m s$^{-1}$, which ultimately led to failure at the bone. Swept wings do not 'flutter', and they avoid static failure by bending and twisting under lift-loads (Fig. 4 top), which reduces the effective angle of attack at the hand-wing and thereby caps aerodynamic load. Such phenomena are not captured by theoretical or experimental studies using rigid wing models[25].

High sweep maximizes high-speed glide performance, but not by creating strong leading edge vortices (LEVs). LEVs have been observed over model swift wings, and have been proposed to boost lift[25]. Our flow visualizations on real wings confirm the presence of LEVs at high sweep angles (≥30°) (Supplementary Table 1). However, our force measurements at speeds of 5–30 m s$^{-1}$ show that swept wings always generated less lift than extended wings. Extra lift from LEVs does not compensate for lift lost to the concomitant drop in wing area and aspect ratio (Fig. 2d, e), and to load-induced wing deformations at high speeds (Fig. 4 top). Sweep improves gliding by decreasing drag, rather than by increasing lift.

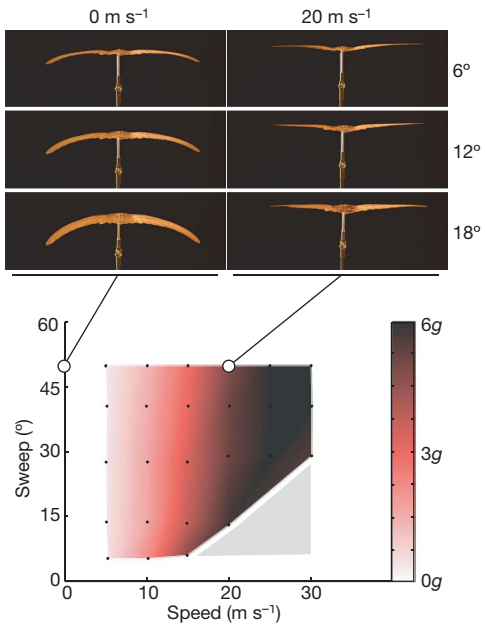


**Figure 4 | Morphing maintains wing structural integrity at high glide speeds.** Bottom: during fast glides, swift wings experience considerable loads (expressed as multiples of *g*; grey, no measurements). Top: swept wings bend and twist under load to a lower angle of attack (rear view; sweep 50°; $\alpha = 6°, 12°, 18°$).

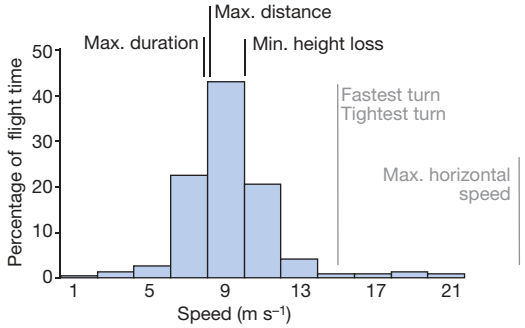


**Figure 5 | Swifts roost at glide speeds that minimize energy expenditure.** Five of six predicted performance maxima occur within the most commonly observed range of flight speeds during roosting[11]: two of three agility-related maxima (grey), and all cost-related maxima (black), which cluster around swifts' preferred roosting speed of 9 m s$^{-1}$.

Our glide model predicts performance-maximizing glide speeds that agree with observations of swift behavioural choices. Glide speeds are readily observable in the field and therefore serve well to validate our semi-empirical glide model. Our model predicts different optimal gliding speeds for maximizing agility (15–25 m s$^{-1}$) versus cost-effectiveness (8–10 m s$^{-1}$). The only glide behaviour on which free-flight data have been published is roosting[11,12,18], for which we expect that flight-cost considerations outweigh agility[11,12]. Radar measurements[11] show that roosting swifts indeed flap-glide at speeds centred around 8–10 m s$^{-1}$ (Fig. 5). This agreement of model predictions and field observations validates the analytical step from wing aerodynamic to bird glide performance.

The modification of glide performance achieved by morphing is comparable to the differences between bird species with widely different wing shapes and flight behaviours[15]. Swifts can adjust their wings' maximum lift coefficients between 0.8 and 1.1, which is similar to the full range from thrush (0.8) to nighthawk (1.15) found[15] for extended wings. Therefore, extended wing geometry alone might not be enough to properly evaluate bird gliding performance[8,15]. Birds with an aerial life style, such as swifts, face a wide range of tasks with sometimes conflicting performance goals. To match wing shape to the task at hand, morphing provides birds with a suite of wing geometries from which to choose.

## METHODS

**Animals.** In spring 2005, we received from eight Dutch bird sanctuaries 35 adult swifts that had died after having been brought in. We selected 15 swifts on the basis of wing state and general state.

**Wing preparation.** We separated 15 wing pairs from the body at the shoulder joint, and manually extended them onto templates for five sweep angles (5°, 15°, 30°, 40°, 50°; Fig. 2a–c). Manually extending wings reliably reproduces wing shape during gliding[26]. Wing pairs were frozen, freeze-dried, then glued together to form a continuous wing surface. They were mounted onto the sting of the balance system and placed in a wind tunnel[27].

**Wind tunnel tests.** We used the Delft low-turbulence wind tunnel[27] with an octagonal test section of 1.80 × 1.25 m (turbulence levels ≤0.025% until 40 m s$^{-1}$). We designed a balance system with a resolution of 40,000 steps to measure lift and drag at air speeds between 5 and 30 m s$^{-1}$ (Reynolds number, 12,000–77,000) with an accuracy of at least 3% (Ohaus SP402). We calibrated the balance with a 5 × 5 matrix of weights over the full lift and drag range to account for the system's small nonlinearity. Each force value was sampled at 5 Hz for 10 s at each angle of attack, $\alpha$ ($0° \rightarrow +30° \rightarrow -6° \rightarrow 0°$; $\Delta\alpha = 1.5°$, precision < 0.5°). Data from the up- and down-leg of the $\alpha$ cycle were pooled, because hysteresis

was negligible below stall. Measurements were corrected for aerodynamic forces of the sting, and for changes in the wings' centre of mass with $\alpha$. To detect the LEV, we moved a tuft (hair from R.K.) along the wing[28].

**Lift–drag polar of swifts.** We built the total lift–drag polar of swifts from wing lift and drag, and body drag. Wing polars were built from force measurements across a range of glide speeds (5–30 m $s^{-1}$), sweeps (5°–50°) and $\alpha$ values ($-6°$ to 30°), excluding high values of $\alpha$ at which the wing stalls—stall was assumed to have occurred when mean lift flattened off and instantaneous lift suddenly became variable. We measured an average body drag coefficient[29] of 0.26 for a frontal area of 913 $mm^2$ (Supplementary Fig. 1).

**Calculation of glide path.** To evaluate the correct part of the total polar, we used a body weight of 43 g (ref. 30) to calculate glide paths. By solving for the unknown parameters glide angle, $\gamma$, bank angle, $\mu$, and turn radius, $R$ (Fig. 1), we obtained equations of motion that contain only measurable quantities—body mass, $m$, body weight, $W$, flight speed, $V$, lift, $L$, and drag, $D$ (Supplementary equations (1)):

$$\begin{pmatrix} \gamma \\ \mu \\ R \end{pmatrix} = \begin{pmatrix} \arcsin\left(\frac{D}{W}\right) \\ \arccos\left(\frac{\sqrt{W^2-D^2}}{L}\right) \\ \frac{mV^2}{W^2}\left(\frac{W^2-D^2}{\sqrt{L^2+D^2-W^2}}\right) \end{pmatrix} \quad (1)$$

We then determined all possible helicoidal glide paths[21] (assuming constant glide speed and no side slip).

**Calculation of performance maxima.** We formulated six figures of merit[21] (Fig. 3): (1) maximum glide distance[21], max($1/\tan\gamma$) (=maximum glide ratio), (2) maximum glide duration[21], max($1/(V\sin\gamma)$), (3) maximum turning angle for a given height loss, max ($1/(R\tan\gamma)$), (4) maximum angular velocity in a turn[21], max($V\cos\gamma/R$), (5) maximum curvature of the turn path[21], max($1/R$), and (6) maximum horizontal component of the flight speed, max($V\cos\gamma$) (Supplementary equations (1)).

We limited the performance analysis by two criteria. First, calculations were only valid for non-zero turning radii (no pure roll around body axis). Second, values for dives (glide angle $\gamma > 45°$) were calculated, but ignored in the search for performance maxima. We linearly interpolated the force coefficients of the two adjacent polars to calculate the 45° dive-angle cut-off speed, straight flight performance maxima, and minimum and maximum flight speeds. Finally, we averaged performance indices per sweep angle to construct Fig. 3 (Supplementary Fig. 2).

**Sensitivity analysis.** The performance maxima occur at the same wing configuration when we change body drag coefficient ($-100\%$, $+200\%$), body weight ($\pm 23\%$) and add the tail's contribution to lift ($\pm 20\%$ of wing lift).

**Accuracy of roost speed prediction.** Air density at the average roosting height[11,18] (1,700 m) was not reported. We measured air density at sea level ($1.201 \pm 0.005$ kg $m^{-3}$), underestimating optimal speed by maximally 9%. However, roosting flight speed does not correlate strongly with altitude (A.H., unpublished observation based on refs 11, 18).

**Received 27 November 2006; accepted 8 March 2007.**


1. Rosén, M. & Hedenström, A. Gliding flight in a jackdaw. *J. Exp. Biol.* **204,** 1153–1166 (2001).
2. Tucker, V. A. Gliding birds: the effect of variable wing span. *J. Exp. Biol.* **133,** 33–58 (1987).
3. Pennycuick, C. J. Gliding flight of the fulmar petrel. *J. Exp. Biol.* **37,** 330–338 (1960).
4. Newman, B. G. Soaring and gliding flight of the black vulture. *J. Exp. Biol.* **35,** 280–285 (1958).
5. Pennycuick, C. J. Wind-tunnel study of gliding flight in the pigeon *Columba livia*. *J. Exp. Biol.* **49,** 509–526 (1968).
6. Müller, U. K. & Lentink, D. Turning on a dime. *Science* **306,** 1899–1900 (2004).
7. Weiss, P. Wings of change: shape-shifting aircraft ply future skyways. *Sci. News* **164,** 359 (2003).
8. Rayner, J. M. V. in *Current Ornithology* Vol. 5 (ed. Johnston, R. F.) 1–66 (Plenum, New York, 1988).
9. Hoerner, S. F. & Borst, H. V. *Fluid-dynamic Lift* (Hoerner, Bakersfield, California, 1985).
10. Azuma, A. *The Biokinetics of Flying and Swimming* 2nd edn (AIAA Education Series, Reston, Virginia, 2006).
11. Bäckman, J. & Alerstam, T. Confronting the winds: orientation and flight behaviour of roosting swifts, *Apus apus*. *Proc. R. Soc. Lond. B* **268,** 1081–1087 (2001).
12. Bruderer, B. & Weitnauer, E. Radarbeobachtungen über Zug und Nachtflüge des Mauerseglers (*Apus apus*). *Rev. Suisse Zool.* **79,** 1190–1200 (1972).
13. Parrott, G. C. Aerodynamics of gliding flight of a black vulture *Coragyps atratus*. *J. Exp. Biol.* **53,** 363–374 (1970).
14. Nachtigall, W. Der Taubenflügel in Gleitflugstellung: geometrische Kenngrössen der Flügelprofile und Luftkrafterzeugung. *J. Ornithol.* **120,** 30–40 (1979).
15. Withers, P. C. An aerodynamic analysis of bird wings as fixed aerofoils. *J. Exp. Biol.* **90,** 143–162 (1981).
16. Thomas, A. L. R. The flight of birds that have wings and tails: variable geometry expands the envelope of flight performance. *J. Theor. Biol.* **183,** 237–245 (1996).
17. Tucker, V. A. & Parrott, G. C. Aerodynamics of gliding flight in a falcon and other birds. *J. Exp. Biol.* **52,** 345–367 (1970).
18. Bäckman, J. & Alerstam, T. Harmonic oscillatory orientation relative to the wind in nocturnal roosting flights of the swift *Apus apus*. *J. Exp. Biol.* **205,** 905–910 (2002).
19. Lack, D. *Swifts in a Tower* (Methuen, London, 1956).
20. Pennycuick, C. J. Flight of auks (Alcidae) and other Northern sea birds compared with Southern Procellariiformes: ornithodolite observations. *J. Exp. Biol.* **128,** 335–347 (1987).
21. Ruijgrok, G. J. J. *Elements of Airplane Performance* (Delft Univ. Press, Delft, 1994).
22. Vogel, S. *Life in Moving Fluids* 2nd edn (Princeton Univ. Press, Princeton, 1994).
23. Schmitz, F. W. *Aerodynamik des Flugmodells* (C.J.E. Volckmann, Berlin, 1942).
24. Schlichting, H. *Boundary Layer Theory* 7th edn (McGraw-Hill, New York, 1979).
25. Videler, J. J., Stamhuis, E. J. & Povel, G. D. E. Leading-edge vortex lifts swifts. *Science* **306,** 1960–1962 (2004).
26. Hedenström, A. & Rosén, M. Predator versus prey: on aerial hunting and escape strategies in birds. *Behav. Ecol.* **12,** 150–156 (2001).
27. Veldhuis, L. L. M. *Configuration and Propulsion Aerodynamics Research in the Low Speed Aerodynamics Laboratory* [in Dutch] (Internal Report LSW 93–1, Faculty of Aerospace Engineering, Delft University of Technology, Delft, 1993).
28. Bird, J. D. *Tuft-Grid Surveys at Low Speeds for Delta Wings* (Technical Note D-5045, NASA, Hampton, Virginia, 1969).
29. Pennycuick, C. J., Alerstam, T. & Hedenström, A. A new low-turbulence windtunnel for bird flight experiments at Lund University, Sweden. *J. Exp. Biol.* **200,** 1441–1449 (1997).
30. Glutz von Blozheim, U. N. & Bauer, K. M. *Handbuch der Vögel Mitteleuropas* (Akademischer, Wiesbaden, 1980).


**Supplementary Information** is linked to the online version of the paper at www.nature.com/nature.

**Acknowledgements** Swifts were supplied by Vogelopvang Woudenberg, Fugelpits Moddergat, Fugelhelling Ureterp, Vogelopvang De Strandloper Bergen, Vogelasiel De Wulp Den Haag, Vogelasiel Haarlem, Vogelasiel Naarden and Vogelopvang Someren. Swift photographs were provided by J.-F. Cornuet (front-view, Fig. 1a) and L.G.M. Schols (side-view Fig. 1a; Fig. 1b). N.G. Verhagen, J. Bäckman and J.H. Becking helped with background research. E.W. Karruppannan, L.J.G.M. Bongers, L. Molenwijk, L.M.M. Boermans, S. Bernardy and H. Schipper helped with the experimental set-up. F.T. Muijres and R. Petie helped with the experiments. T.P. Weber and S.M. Deban critically read the manuscript. O. Berg improved many versions of the manuscript. U.K.M. is funded by NWO, and A.H. by Carl Trygger's Foundation.

**Author Information** Reprints and permissions information is available at www.nature.com/reprints. The authors declare no competing financial interests. Correspondence and requests for materials should be addressed to D.L. (david.lentink@wur.nl).